CHEMISTRY OF MATERIALS

Open Access

pubs.acs.org/cm

Article

The Influence of Residual Copper Catalyst on the Polymer-to-Ceramic Conversion of a Click-Derived Polycarbosilane

James F. Ponder, Jr,[○] Haira G. Hackbarth,[○] Stephanie L. Chua, Yuwei Yang, Nicholas D. Posey, Brandon J. Ackley, Chih-Wen Pao, Andrey A. Yakovenko, Matthew B. Dickerson,* Nicholas M. Bedford,* and Timothy L. Pruyn*

Cite This: *Chem. Mater.* 2026, 38, 3941−3950

Read Online

ACCESS | Metrics & More | Article Recommendations | Supporting Information

ABSTRACT: Preceramic polymers (PCPs) are a key class of materials for the preparation of advanced ceramic components. Following conventional polymer processing and subsequent pyrolysis, polymer-derived ceramic (PDC) fibers, monoliths, and composites offer novel engineering opportunities for aerospace applications. Despite the rapidly emerging commercial applications of PDCs, many basic scientific questions remain regarding the structural transformation of the polymer to the final ceramic and how processing variables affect PDC materials properties. PCPs prepared using a mild and scalable copper (Cu) catalyzed azide/alkyne "click" reaction have been demonstrated as a unique class of material that can bind with transition metals, ultimately producing ultrahigh temperature ceramics (UHTCs) upon pyrolysis. Unexpectedly, it was found that the removal of residual Cu catalyst from a model click-derived polycarbosilane PCP significantly reduced the ceramic yield during pyrolysis. Herein, we report the influence of Cu impurities on polycarbosilane-derived SiC ceramics and present a mechanistic understanding of the unintended role of Cu in the polymer-to-ceramic conversion process. Synchrotron-based scattering and spectroscopy methods were implemented to track the evolution of different atomic species and local structures as well as the influence of Cu toward atomic-scale structures in the final ceramics. It was determined that Cu impurities catalyze the formation of silicon carbide through the formation of an intermediate molten copper/copper silicide, ultimately increasing the ceramic yield. Overall, this contribution highlights the need to carefully assess the interplay between the chemistries needed for PCP synthesis and their potential influence on final PDCs following processing.

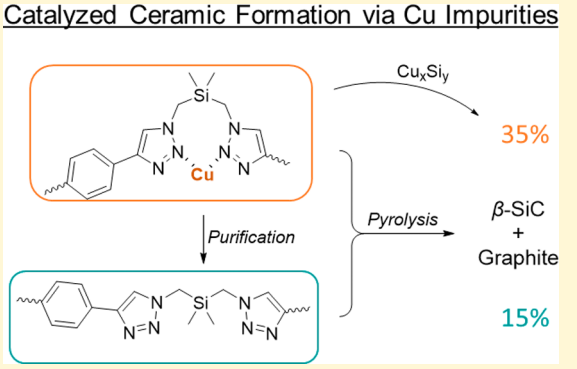

1. INTRODUCTION

Preceramic polymers (PCPs) allow for the production of advanced ceramic materials, offering the desirable processability and synthetic tunability of polymers with the ability to form ceramic components upon pyrolysis.[1−4] The morphology and composition of the resulting polymer derived ceramic (PDC) are dependent on both the initial PCP chemistry/structure/morphology and the curing/pyrolysis conditions.[5] Currently, there have been insufficient studies to decouple these variables and generate robust structure-processing-product relationships. While substantial work has been done utilizing commercial Si-based polymers, development of new materials using modern synthetic methods is an area of great interest in the field.[2,6] Currently, the most common polymerization methods used to prepare PCPs (e.g., Kumada, hydrosilylation) exhibit poor reaction control, leading to largely inconclusive outcomes for a material design and processing perspective.[2]

In recent years, the class of synthetic methods known as "click" reactions have gained popularity in materials science, ultimately leading to the 2022 Nobel Prize in Chemistry being awarded for their development.[7] Click reactions simultaneously provide reaction selectivity, high synthetic yield, as well as tolerance of functional groups and solvent conditions.[6,8] Among the various click reactions, thiol-ene and thiol-yne reactions are prominent due to their utilization for polymer functionalization and cross-linking.[9−11] Another strategy involves the utilization of nitrogenous systems. For example, the copper (Cu) catalyzed azide/alkyne click reaction to form nitrogen-based triazoles is a promising route to yield PCP materials which can, upon pyrolysis, either lose nitrogen as N_2 or incorporate it into the PDC.[6,12,13] It has been demonstrated via X-ray crystallography that Cu atoms can coordinate between the nitrogen lone pairs of two triazole units.[14,15] This ability to coordinate transition metals has been utilized to

Received: October 22, 2025
Revised: March 2, 2026
Accepted: March 5, 2026
Published: April 13, 2026

Scheme 1. a) The Synthetic Route for Preparation of the Different cPCP Batches; (b) an Illustration of Possible Copper Complexes along (Intra) or between (Inter) Polymer Chains, we note that while the Proposed Inter-Chain Chelation Structure is More Favorable due to the Relatively Higher Electron Richness of the N_3 Nitrogen,[17] Prior Crystallographic Results are More Comparable to the Intra-chain Structure;[14,15] (c) the Structure of EDTA-K_2

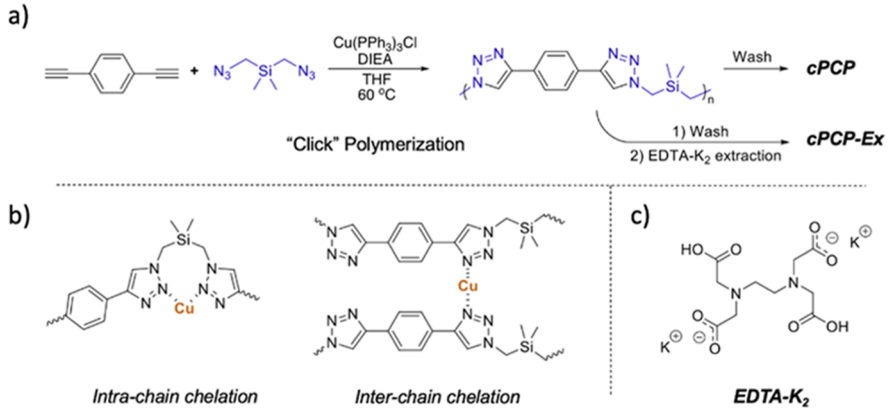

form metal carbide (e.g., ZrC) upon pyrolysis, providing an attractive route for the synthesis of ultrahigh temperature ceramics (UHTC).[6,16]

The azide/alkyne click reaction of 1,4-diethynylbenzene and bis(azidomethyl)dimethylsilane, shown in Scheme 1a, to yield a polycarbosilane (PCS) has been previously reported by Bouzat and co-workers.[6] In this initial study, the authors emphasized that the synthesized polymer was produced without any attempts to remove the Cu contaminant. As 1,2,3-triazoles have been demonstrated to effectively coordinate Cu, a matter that will be discussed further in the text, it is expected that some amount of Cu from the polymerization will be trapped,[15] as illustrated in Scheme 1b. Upon pyrolysis at 1500 °C, the authors report an unexpected α-SiC phase with copper silicide (Cu_xSi_y) impurities.[6] However, the published X-ray diffraction (XRD) spectrum shows, predominately, peaks corresponding to β-SiC, suggesting inconsistencies in the phase assignment.[6] In a subsequent report, the authors attempted to remove residual copper catalyst from the PCS by washing it with aqueous ammonia.[16] Following pyrolysis at 1400 °C, the resulting material was determined to consist of β-SiC with Cu_xSi_y impurities, highlighting the challenge of the complete removal of Cu from this system. From these reports, it remains unclear if the formation of α-SiC occurs in this click derived PCS, and if so, whether it is a result of the specific polymer structure or residual Cu in the system.[16] Regardless of the SiC polymorph formed, the role and evolution of residual Cu on the ceramization process of the PCP remain an open question, one that requires further clarity, as click-derived PCPs become increasingly researched in the community.

In this work, we have investigated the influence of residual Cu in the polymer-to-ceramic conversion of a previously reported model click-derived PCP, denoted here as cPCP (Scheme 1a). Following the synthesis and filtration/washing of cPCP, a portion of the materials was additionally extracted with a dipotassium ethylenediaminetetraacetic acid (EDTA-K_2, Scheme 1c) solution to bind to Cu ions[18,19] and remove them from the polymer, resulting in a sample termed cPCP-Ex, as outlined in Scheme 1a. In addition to standard ceramic characterization methods, synchrotron-based techniques were utilized to reveal more detailed atomic-scale understanding with high spatial resolution.[20] Specifically, total synchrotron scattering, combined with atomic pair distribution function (PDF) analysis, was utilized as it is a powerful tool to investigate the local structure of PCPs and PDCs.[21,22] Furthermore, using X-ray spectroscopy methods, chemistry and structure information was probed in an element-specific fashion.[23] Such understanding is valuable for comprehending the nearest-atomic neighbor arrangement, particularly regarding the influence of Cu species in the ceramization of click-derived polymers. Our efforts provide a mechanistic understanding of the effect of often ignored residual polymerization catalyst and highlight the importance of not only polymer structure but also purification methodology on the resulting ceramic.

2. RESULTS AND DISCUSSION

2.1. Polymer Synthesis and Purification

The model PCS, cPCP, was synthesized via an azide−alkyne click polymerization, as seen in Scheme 1a, using $(PPh_3)_3CuCl$ as the catalyst. The polymer was subsequently precipitated and washed with hexanes and isopropyl alcohol (IPA), resulting in a polymer batch termed cPCP. A portion of cPCP was then suspended in dichloromethane (DCM) and washed and extracted with an aqueous EDTA-K_2 solution to remove Cu. The DCM layer was isolated and dried to yield cPCP-Ex. Full synthetic details, as well as additional discussions of alternative workup conditions and catalysts, are given in the Supporting Information.

Residual copper levels in the polymer samples were quantified by inductively coupled plasma optical emission spectroscopy (ICP-OES) and inductively coupled plasma mass spectrometry (ICP-MS) for cPCP and cPCP-Ex, respectively. Measurements were performed by Galbraith Laboratories, Inc., with sample preparation and analysis details provided in the Supporting Information. The cPCP was found to contain 2.28% Cu by weight (1.00 Cu atom per 400. triazole rings), with EDTA extraction lowering the concentration to 0.21% for cPCP-Ex. This 10x reduction in Cu levels, while lower than expected from the extraction, results in all the further changes reported in the following sections as no change in molecular weight or structure occurs from the extraction method.

2.2. Gravimetric and Initial Crystallographic Analysis

Thermogravimetric analysis (TGA) was used as the first comparison of cPCP and cPCP-Ex. As seen in Figure 1, no

https://doi.org/10.1021/acs.chemmater.5c02801
Chem. Mater. 2026, 38, 3941−3950

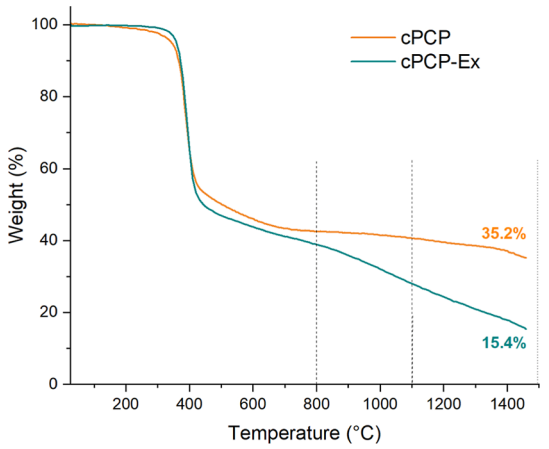

Figure 1. TGA of pristine cPCP and after extraction with EDTA (cPCP-Ex). Dashed lines denote temperatures of interest for further analysis.

significant differences between the samples are observed until ~420 °C, at which point cPCP-Ex initially loses only slightly more mass than cPCP. cPCP-Ex continues to lose mass at a steady rate until the final temperature of ~1500 °C, with a corresponding char yield of 15%. Alternatively, the mass loss of cPCP reduces in magnitude between 730 and 1500 °C, resulting in a char yield of 35%. The significant decrease in char yield after the removal of Cu in cPCP-Ex suggests that it plays a crucial role in the retention/conversion of material during pyrolysis. We note that the theoretical ceramic yield from this polymer is 13.5% for pure SiC formation and 37.8% for a mixture of SiC and graphite, with the TGA measured yields indicating we have produced the latter composition. To further confirm that the presence of Cu is responsible for the higher ceramic yield, we have reintroduced Cu into cPCP-Ex via dissolution of the polymer and $(PPh_3)_3CuCl$ complex in DCM, followed by mixing overnight and drying, with full details outlined in the Supporting Information. As seen in Figure S1, the reintroduction of Cu significantly increased the ceramic yield of cPCP-Ex, with a 1% Cu catalyst complex introduction leading to an ~15% increase (a doubling) of ceramic yield. We note that this increase is larger than expected base on the measured Cu levels in cPCP and cPCP-Ex, indicating the exact form of Cu (e.g., a well dispersed metal complex vs Cu nanoparticles), oxidation state (0, I, or II), and degree of dispersion within the polymer matrix may influence the degree of char yield enhancement and will require further research.

XRD measurements were performed on pyrolyzed samples of cPCP and cPCP-Ex to assess the basic composition of the resulting PDCs. In addition to pyrolysis at 1500 °C, samples were also prepared at intermediate temperatures of 800 and 1100 °C (see dashed lines in Figure 1) in an effort to elucidate the changes that ultimately result in significant differences in ceramic yield. As shown in Figure 2a, a crystalline phase is observed with peaks that can be best fitted to elemental Cu (PDF 00-004-0836) for both samples after pyrolysis at 800 °C. An amorphous phase at an angle of ~25° can also be observed, along with some small peaks that could not be definitively assigned. Pyrolysis at 1100 °C (Figure S2) results in relatively few changes as observed by XRD, with a sharpening of the crystalline peaks for both samples and reduction of peak intensity for the amorphous phase of cPCP. At the final

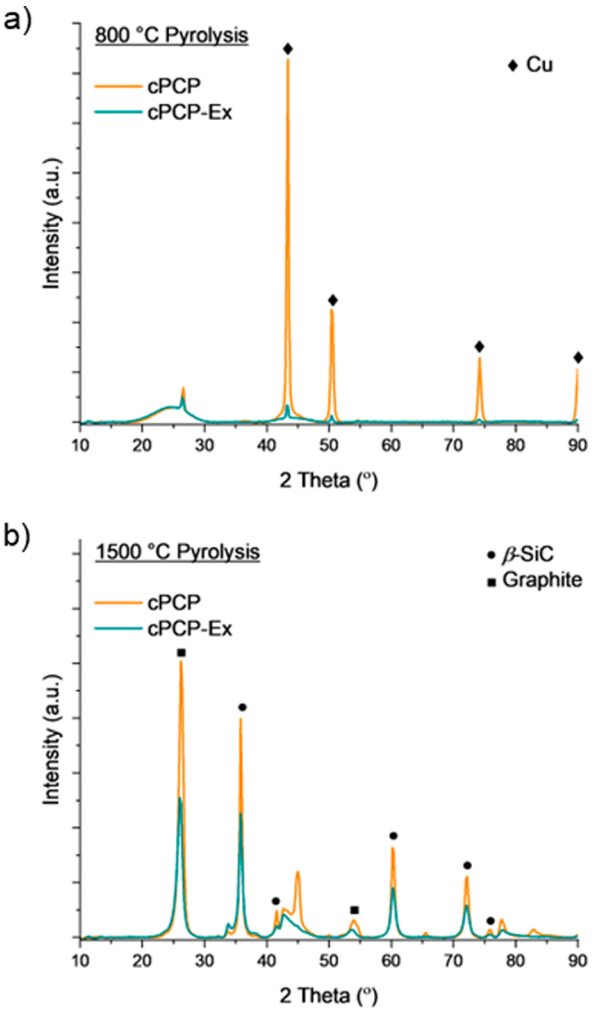

Figure 2. XRD patterns of cPCP and cPCP-Ex samples that have been pyrolyzed in Ar at (a) 800 and (b) 1500 °C.

pyrolysis temperature of 1500 °C (Figure 2b), a completely different set of crystalline phases are observed, with the Cu phase disappearing and replaced by a mixture of β-SiC and graphite.

2.3. Post-Pyrolysis Morphological and Compositional Analysis

Scanning electron microscopy (SEM) with energy dispersive X-ray spectroscopy (EDS) was utilized to qualitatively assess the domains of residual Cu species seen in the PDC samples. Samples pyrolyzed at 800 and 1100 °C were found to be generally comparable, with the 1100 °C samples being discussed for illustration. For samples of cPCP, teardrop-shaped copper containing inclusions were readily observed across the powder (Figure 3a), and with higher magnification of a selected area shown in Figure 3b, visible intermediate amounts of copper inclusions were readily detected that were consistent across all sampled areas. The EDS mapping of this area (Figure 3b) reveals that the teardrop was composed primarily of Cu, with a weaker signal of Si, potentially indicating the inclusion of a Si-based species or Si doping of Cu (e.g., Cu_xSi_y) rather than simply pure elemental copper. Qualitatively, cPCP-Ex had less detectable surface copper remaining in the powder (i.e., Cu was not frequently encountered) compared to cPCP, as seen in the representative

https://doi.org/10.1021/acs.chemmater.5c02801
Chem. Mater. 2026, 38, 3941−3950

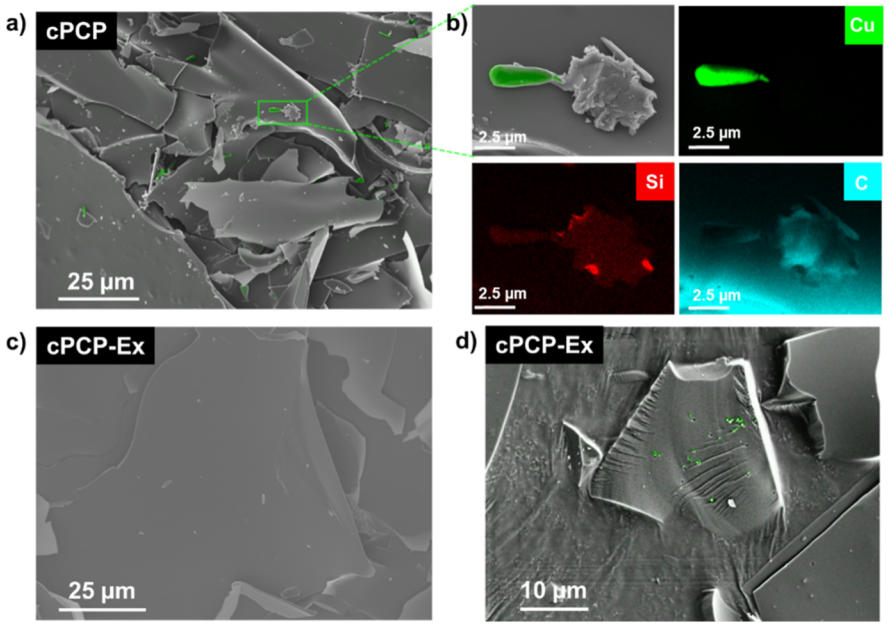

Figure 3. Representative SEM micrographs/EDS map of samples pyrolyzed at 1100 °C. (a) cPCP with (b) selected area for EDS elemental maps of copper (green), silicon (red), and carbon (blue). (c) SEM micrograph of cPCP after EDTA-based extraction, with residual copper detected in some instances, (d) as shown in magnified SEM images.

area of Figure 3c. EDS of the areas shown in Figure 3a,c are overlaid in Figure S3 (see Supporting Information) and further illustrate difference in copper levels between the two. In rare cases (Figure 3d), trace copper was still detectable while scanning cPCP-Ex samples. This is consistent with ICP measurements demonstrating a significant reduction, but not totally elimination, of Cu by the EDTA extraction, with an example of trace Cu impurities in cPCP-Ex shown in Figures 3d and S4.

Following pyrolysis at 1500 °C, both cPCP and cPCP-Ex samples had detectable surface copper (Figures S5 and S6), despite the disappearance of the crystalline Cu peaks from the XRD patterns. cPCP samples had easily identified distinct copper inclusions, as shown in Figure S5, although other large areas had varying amounts of copper. The Cu hot spot signals are colocalized with faint silicon signals but are mostly disparate features embedded in a granular silicon and carbon-rich matrix, comparable to what was observed in 1100 °C samples. In contrast, cPCP-Ex samples had a distinctly weaker Cu signal compared to Si (Figure S6). Overall, qualitative SEM EDS measurements are consistent with ICP measurements, showing that while the EDTA extraction did reduce the amount of Cu in the samples, it did not fully remove it. In several cases, Si and Cu were observed as colocalized, indicating the possible presence of a Cu_xSi_y phase.

2.4. Spectroscopic Analysis

To gain insights into the surface chemistry and coordination environments of Si and Cu, X-ray absorption spectroscopy (XAS) measurements were performed on materials pyrolyzed at 800, 1100, and 1500 °C. The Si K-edge X-ray absorption near edge structure (XANES) spectra for cPCP and cPCP-Ex are shown in Figure 4a,b, respectively. The main feature in both spectra at 800 and 1100 °C is the prominent peak at 1848 eV, similar to that found in SiO_2 and Cu_xSi_y intermediates, as comparatively measured from standard samples of SiO_2 and Cu_5Si (Figure S7a,b).[24,25] The presence of silica potentially

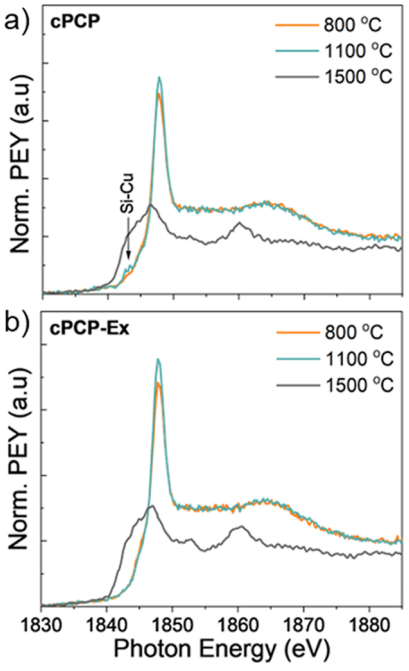

Figure 4. NEXAFS measurements at the Si K-edge of (a) pristine cPCP and (b) after extraction with EDTA (cPCP-Ex).

results from surface oxidation or residual air during vacuum oven curing. We note that due to the electron yield measurement modality used for Si K-edge measurements, this methodology is itself surface sensitive and could emphasize any surface oxidation. A discrete feature at ~1841 eV is seen for cPCP at 1100 °C (Figure 4a) and is assigned to the electronic transition from Si 1s to an unoccupied metal−adsorbate band. This observation suggests that an Cu−Si intermediate exists alongside SiO_2 at this intermediate temperature, and only specific for cPCP since it contains a substantial amount of copper to promote this interaction.[25]

https://doi.org/10.1021/acs.chemmater.5c02801
Chem. Mater. 2026, 38, 3941−3950

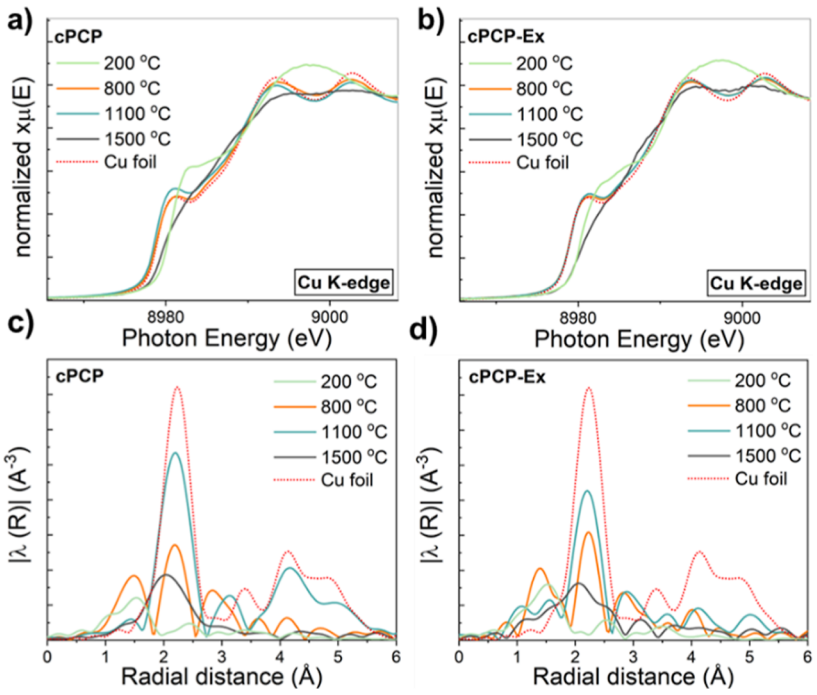

Figure 5. Cu K-edge XANES spectra of (a) cPCP and (b) cPCP-Ex pyrolyzed at 200, 800, 1100, and 1500 °C. Fourier-transformed (FT) EXAFS spectra of (c) cPCP and (d) cPCP-Ex.

Regardless of the initial composition, both cPCP and cPCP-Ex samples exhibited features associated with β-SiC after pyrolysis at 1500 °C, as seen in Figure 4 and more closely compared against a known standard in Figure S7c. This observation is substantiated by our near-edge X-ray absorption fine structure (NEXAFS) measurements of the C and N K-edges found in Figure S8. The C K-edge data showcases an increase in C−Si character at higher pyrolysis temperatures, along with associated carbon phases that are present in the PDC.[26,27] Furthermore, there is notable C−N contributions, which are also observed in the N K-edge and indicate the presence of pyridinic N−C in the carbon matrix.[28,29] Importantly, the N K-edge NEXAFS does not resemble those for Si−N based materials,[30] strongly indicating the presence of a predominate SiC ceramic phase.

The local atomic structure and coordination of Cu were likewise monitored in cPCP and cPCP-Ex. Figure 5a,b show the Cu K-edge XANES spectra after thermal processing (curing or pyrolysis) at 200, 800, 1100, and 1500 °C, where the inclusion of the cured material at 200 °C is probed to verify the initial state of Cu in these materials. At the initial cure state, cPCP (Figure 5a) exhibited peaks at 8982.7 and 8997.2 eV that are consistent with a Cu (I) oxidation state.[31,32] The cPCP-Ex showed a similar profile, demonstrating a similar local environment of Cu (I) in the cure state for both materials. As the processing temperatures increase, the XANES profiles (Figures 5a and S9) of cPCP and cPCP-Ex resemble that of the Cu foil, with features assigned to the 1s to 4p transitions and the doublet at higher energy characteristic of metallic Cu, indicating reduction of Cu (I) to Cu (0) species.[31,33−35] On closer inspection, we observed that the rising edge of cPCP at 1100 °C is higher in intensity than its 800 °C counterpart, indicating a higher electron population in the Cu d-orbitals of cPCP originating from the Si−Cu interactions seen in the Si K-edge spectrum at 1100 °C (Figure 4a). We hypothesize that molten metallic Cu (melting point = 1085 °C) diffuses into the Si−O bonds in cPCP due to the high diffusion coefficient of Cu in Si at those temperatures, giving rise to an intermediate Cu−Si phase, ultimately observed at ambient conditions as a copper silicide phase.[35,36] Meanwhile, there was no change in the XANES features at low and intermediate temperatures for cPCP-Ex. As SiC is seen forming at higher temperatures from Figure 4, the Cu K-edge reveals that cPCP and cPCP-Ex both reverted a mix of Cu and Cu_2O states after silicide catalyzed conversion to the ceramics, wherein the exposed metallic Cu becomes partially oxidized in this environment. Additionally, we note that the characteristic signatures for Cu−C and Cu−N interactions[37,38] are not observed in these samples.

The Fourier-transformed extended X-ray absorption fine structure (EXAFS) oscillations for cPCP and cPCP-Ex after pyrolysis at 1500 °C are shown in Figure 5c,d, respectively. The k^2-weighted EXAFS plots (not phase corrected) are shown in Figure S9. Copper foil has a main peak at ∼2.3 Å, which is attributed to the Cu−Cu bond. For cPCP and cPCP-Ex cured at 200 °C, a peak at ∼1.5 Å is present, corresponding to a Cu−O coordination.[31,32] At 800 °C, the spectra of both samples exhibit features of both Cu−O and Cu−Cu coordination at ∼1.5 and ∼2.3 Å (not phase corrected), respectively, reflecting a mixture of Cu states, noting that the Cu−O distance can be a contribution of copper oxide and chelated Cu species. From 1100 °C onward, both materials have a primary feature at ∼2.3 Å that is associated with coordination spheres in metallic Cu and Cu_5Si, wherein both materials have similar local Cu structure.[25,32,39] A higher Cu−Cu intensity for cPCP is similarly observed, indicating a higher local coordination environment that likely resembles a bulk material, given the higher concentration of Cu. Upon pyrolysis at 1500 °C, the two materials displayed prominently different spectra from one another. The reappearance of a shorter first coordination sphere is evident in cPCP-Ex (∼1.5 Å) that is missing in cPCP, while both materials exhibit a diminished Cu—metal coordination sphere that is slightly smaller as

https://doi.org/10.1021/acs.chemmater.5c02801
Chem. Mater. 2026, 38, 3941−3950

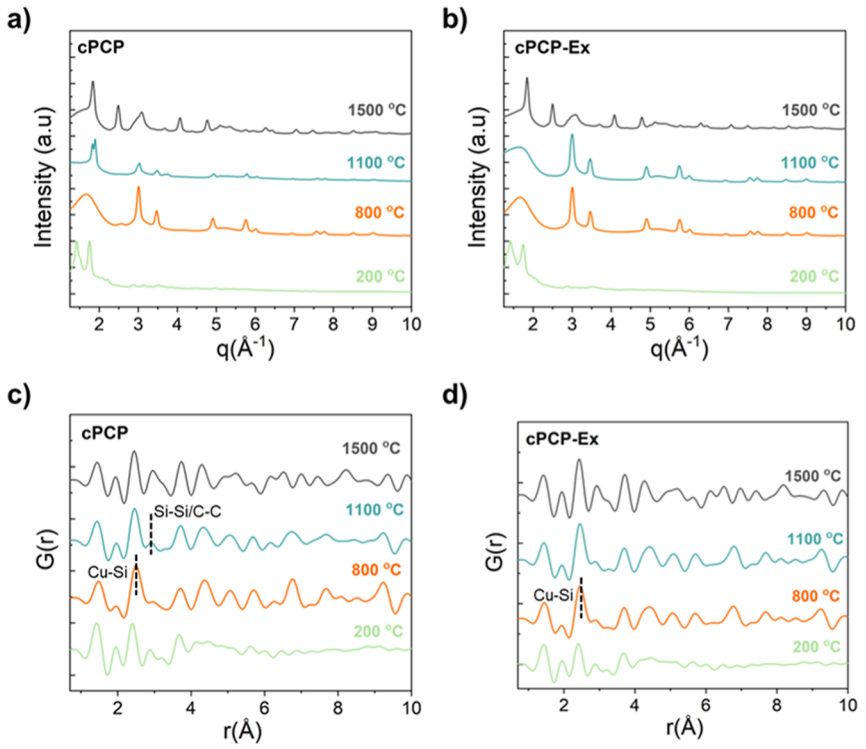

Figure 6. Resulting HE-XRD patterns and atomic PDFs up to 10 Å correlation of (a,c) cPCP and (b,d) cPCP-Ex.

compared to similar features at lower pyrolysis temperatures. In addition, the Cu—metal distances in cPCP exhibit shoulder features that are not present in PCP as well. Given the large Cu concentration difference between cPCP and cPCP-Ex, the Cu K-edge EXAFS indicates that the residual Cu in cPCP likely forms metallic aggregates that cannot nucleate and grow as well in cPCP-Ex, leading to mixtures of metallic Cu and oxidized Cu species.

2.5. PDF Analysis

To gain more detailed structural insights into the influence of residual Cu catalysts in the formation of PDCs, high-energy X-ray diffraction (HE-XRD) coupled to atomic PDF was performed on cured and pyrolysis samples of our click derived polymer. PDF analysis incorporates both Bragg and diffuse scattering data from HE-XRD patterns, often referred to as total scattering, providing atomic-scale structural information that includes ordered and disordered phases of a material.[20] Figure 6a,b show the total scattering patterns—collected ex-situ—of cPCP and cPCP-Ex, with corresponding total structure functions ($F(Q)$) displayed in Figure S10.

The absence of significant features in the HE-XRD patterns for both cPCP (Figure 6a) and cPCP-Ex (Figure 6b) at a cured state of 200 °C demonstrates the broadly amorphous nature of the preceramic materials, with the signals detected at low Q (1.42 and 1.75 Å^{-1}) ascribed to locally ordered domains (e.g., $\pi-\pi$ interaction of triazole units) in the PCPs.[40−42] Patterns of SiO_2 and SiC phases start to appear after 800 °C treatment, and structural reorganization is further realized at 1100 °C with a pair of peaks centered at 1.86 Å^{-1} that are exclusively observed in cPCP. These peaks potentially correspond to the graphitic phase observed in the powder XRD analysis and was similarly discerned by C K-edge NEXAFS (Figure S8).[43,44] The characteristic β-SiC features finally emerged at 1500 °C, with diffraction peaks at 3.69 and 4.07 Å^{-1}. We can additionally confirm that hexagonal SiC (6H-polytype) is not present in the resulting ceramics due to the absence of the distinct three-peak profile for this polymorph. In general, the HE-XRD results obtained align with our Si K-edge XANES, which tell us that the formation of SiC is complete at 1500 °C.

The ex-situ atomic PDFs of cPCP and cPCP-Ex post pyrolysis are presented in Figure 6c,d, with the full atomic PDFs that extend to 30 Å presented in the Supporting Information (Figure S10). This technique proves a valuable route to elucidate the unresolved, amorphous diffraction peaks from our previous PXRD and HE-XRD results. After curing, both materials exhibited peaks at 1.42 and 2.4 Å that correspond to Cu−O and Cu−Cu phases, along with possible overlap with low Z atomic pairs in the carbonaceous materials, which align well with our Cu K-edge EXAFS results.[31,32,45,46] Note that while the concentration of Cu is small, its higher atomic mass will contribute more to X-ray scattering, which is reflected in subsequent PDFs. As the processing temperatures increase, additional atomic pairs become more prevalent, indicating the presence of longer-range atomic ordering. We noted that there is a pronounced peak shift from the 2.38 Å peak at 200 °C to 2.47 Å at 800 °C for cPCP and cPCP-Ex. This peak is assigned to Cu−Si pairs in copper silicide, aligning with the EXAFS distances of copper silicide phases at 2.46 Å.[25] Interestingly, the presence of this copper silicide material readily led to the rapid formation of Si−Si/C−C phases, as manifested by the peak at 3.08 Å at 1100 °C in cPCP and becomes intense at 1500 °C. Conversely, SiC from cPCP-Ex only appears after high temperature pyrolysis. This observation, along with our Si and Cu K-edge results, suggests that cPCP readily forms a Cu−Si intermediate that accelerates SiC formation and returns to a Cu_2O phase following high temperature pyrolysis. In contrast, cPCP-Ex may form a transient Cu−Si intermediate that is subsequently lost as the temperatures are increased. Additionally, the production of SiC

https://doi.org/10.1021/acs.chemmater.5c02801
Chem. Mater. 2026, 38, 3941−3950

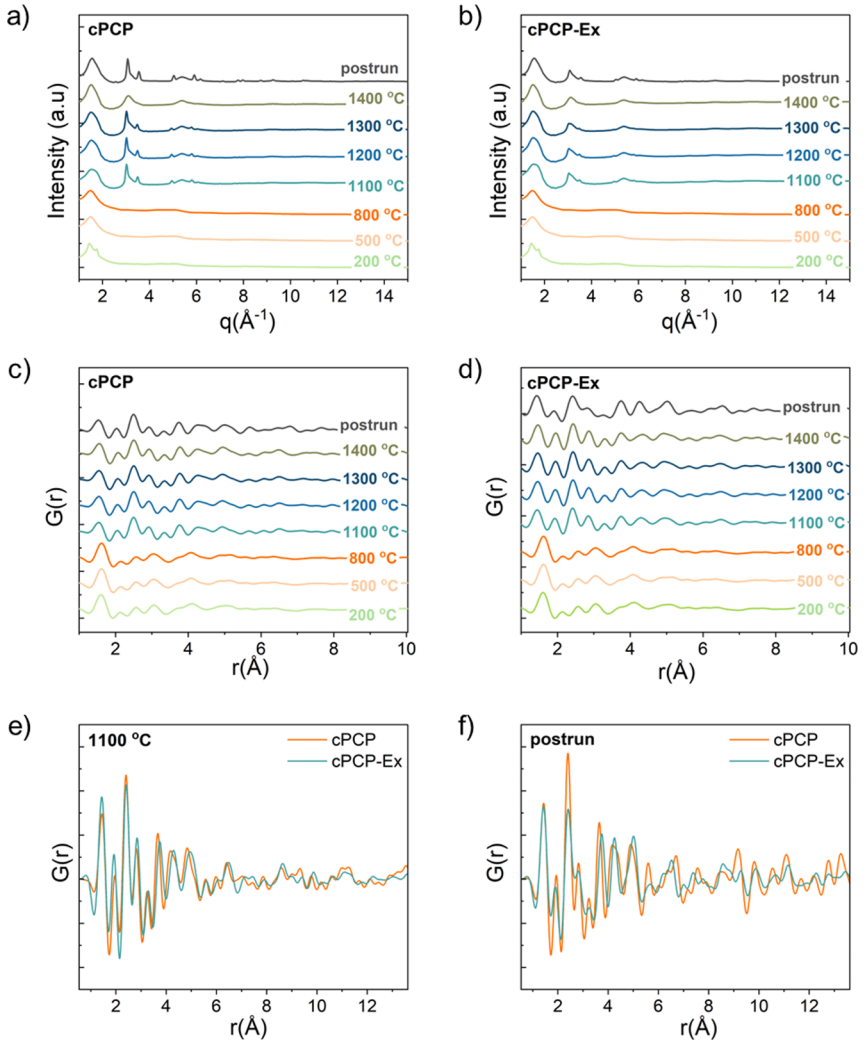

Figure 7. a,b) HE-XRD patterns and (c,d) atomic PDFs at 10 Å of cPCP and cPCP-Ex pyrolyzed under in situ conditions from 200 to 1400 °C, along with a postrun scan following cooling down. Atomic PDFs comparing cPCP and cPCP-Ex under in situ heating at (e) 1100 °C and (f) following cooling, highlighting the peak at 2.48 Å and the broken lines are assigned to Si−Si/C−C reflections.

ceramics from cPCP-Ex may be driven by high temperature carbothermal reduction of the previously discussed Si−O bonds, whereas SiC obtained from cPCP is catalyzed by Cu via mediation of the Cu−Si phase. At the final temperature of 1500 °C, both materials display well-defined peaks due to increased local ordering, where peaks at 1.45, 3.08, and 3.62 Å correspond to graphitic phases and Si−Si/C−C. and Si−C atomic pair distances from SiC.

A comparative analysis of the atomic PDFs of cPCP and cPCP-Ex is presented in Figure S11 and demonstrates that there is an enhanced local ordering of cPCP materials despite no major differences in the PDFs of the pyrolyzed materials before and after Cu extraction. This phenomenon was consistent across all temperatures. Loughney et al. also reported an enhanced crystallization in a commercial polysiloxane matrix when copper nanofiller was incorporated. The authors attributed the formation of Cu−Si intermetallic species to a lower critical nucleation temperature for SiC formation.[47] With the aid of total scattering experiments, we were able to determine that the retention of Cu in a PCP material promotes an ordered SiC formation.

Our PDF results revealed that Cu−Si phases from cPCP aid with the formation of ordered ceramics. To gain additional insights into the ceramic formation process, we employed an in situ pyrolysis setup to capture changes in local ordering during ceramic formation. These measurements were conducted by using two distinct setups to address the challenges of weight loss and volumetric contraction upon pyrolysis. A flow cell capillary furnace[48] was utilized for measurements below ∼1000 °C, while a Linkam stage was employed to reach temperatures up to ∼1400 °C. Comprehensive information regarding data acquisition and setup information can be found in the Supporting Information, where photographs of the instrumentation setup are shown in Scheme S1.

The HE-XRD patterns acquired in situ are presented in Figure 7a,b for cPCP and cPCP-Ex, respectively. Both materials remain unaffected while being heated from 200 to 800 °C (see Figure S12), with signals from low q values originating from the initial polymeric structure and SiO_2-rich phases, as previously discussed in the context of ex-situ measurements.[43,44] The diffraction patterns emerging for both cPCP and cPCP-Ex at 1100 °C do not appear to be significantly different from our ex-situ HE-XRD results. The only notable difference is that the peaks coming from cPCP are better resolved than those from its extracted counterpart, suggesting a well-ordered initial structure likely aided by the

https://doi.org/10.1021/acs.chemmater.5c02801
Chem. Mater. 2026, 38, 3941−3950

presence of Cu−Si phases at elevated temperatures that are missing once the material is cooled back to room temperature. The broad peak at low q values for samples heated at higher temperatures (1100 to 1400 °C) is ascribed to the amorphous carbon phase.[44] The materials were seen to stabilize upon subsequent cooling (labeled as post run) and revert to their original structures in 1100−1300 °C.

The corresponding atomic PDFs from the in situ heating are presented in Figure 7c,d, where the total structure functions and full atomic PDFs up to 30 Å correlation can be seen in Figure S12. Both materials show strong peaks at 1.6 Å from 200 to 800 °C heating, likely from the interatomic distances of Si−O and may contain overlapped contributions from the neighboring C−C atomic pairs.[44] We saw more atomic pairs emerging after subsequent heat treatment from 1100 to 1400 °C likely arising from structural reorganization, which is similar to observations from the ex-situ sample analysis. When we compared the individual in situ PDFs of cPCP and cPCP-Ex at select temperatures in Figure 7e,f. They exhibited similar interatomic distances with their ex-situ counterparts, although we were able to discern more local ordering differences between the samples from the ex-situ conditions, likely due to the longer time at high temperature. Moreover, we also detected the Cu−Si peak at 1100 °C from cPCP and cPCP-Ex at 2.48 Å, with the former sample displaying a more intense peak in cPCP after cooling. It is worth noting that we do not expect complete formation of SiC during the in situ experiments due to the limited time the specialized equipment can be held at the temperatures required for full conversion; however, the transition from SiO_2 to SiC was still sufficiently captured in both materials. Thus, it can be demonstrated that while Cu−Si phases can be formed in both PCP materials, a sufficient amount of Cu must be present to realize its catalytic role and facilitate the production of ordered SiC ceramics.

3. CONCLUSIONS AND PERSPECTIVE

In summary, we have performed comprehensive characterization efforts to track the evolution of different atomic species in Cu-catalyzed click-derived preceramic materials during the ceramization process. From these efforts, we have confirmed the presence of a residual copper effect in the ceramization process of Si-based polymers and elucidated mechanistic details of this newly found effect. Furthermore, we developed a method to investigate the pyrolysis of preceramic polymers under in situ conditions, taking into account the mass loss during heating. Specifically, we used the operational capabilities of two different heating setups to ensure that samples remained within the beam zone during the measurements. This method serves as a foundation for further in situ investigations of PDCs to be utilized in future studies.

While residual catalyst remaining in polymers following synthesis is typically considered a potentially harmful impurity and can present challenges for removal, our results reveal that leaving Cu species in our click-derived system can be uniquely beneficial. Overall, we observed an enhanced mass yield following pyrolysis in ceramics containing higher levels of Cu, with ∼2% Cu leading to an ∼20% increase in yield. This is attributed, at least in part, to the catalytic diffusion of molten Cu into Si−O, which forms intermediate Cu−Si phases from 800 to 1100 °C, observed as Cu_xSi_y upon cooling. Such intermediates facilitate the release of O- and N-containing species that otherwise would be retained in the Si-based matrix or lead to the loss of volatile Si-based species. Simultaneously, we observed a facilitated graphitization of sp2 carbon in higher Cu content samples. At 1500 °C, Cu reverts to its initial oxidized state, while Si species rearrange to form SiC. Under in situ conditions, we observed a persistent SiO_2-rich environment where the segregated carbon remains in an amorphous configuration, preventing the local ordering of the final ceramics compared to ex-situ results. In both conditions, Cu plays an important role in the formation of the SiC phase. Ultimately, we have established that when designing and preparing preceramic polymers, especially those derived from copper-catalyzed click reactions, the influence of residual catalyst, and whether it should be removed, must be considered for control of final yield, ceramic phases, and local ordering.

4. EXPERIMENTAL METHODS

4.1. Polymer Synthesis

cPCP was prepared via an adapted method[6] and was subsequently converted to cPCP-Ex via extraction with EDTA-K_2, with full details in the Supporting Information.

4.2. Bulk Curing and Pyrolysis

Samples were cured in a vacuum at 200 °C for 1 h with a heating rate of ∼1 °C/min. For pyrolysis, samples were placed in Grafoil boats in an alumina crucible and loaded into an alumina tube furnace fitted with a graphite sleeve. Samples were pyrolyzed under Ar by heating from ambient temperature to 800, 1100, or 1500 °C at a heating rate of 10 °C/min and then holding at temperature for 3 h before cooling. Note: while the use of a graphite sleeve in the tube furnace assists in scavenging oxygen, thereby limiting oxidation, it lowers the true temperature of the sample by 40−50 °C at higher temperatures, leading to an actual pyrolysis temperature closer to ∼1460 °C.

4.3. Thermogravimetric Analysis

TGA measurements were collected on a NETZSCH STA 449F3 instrument controlled by X software. Samples were loaded into Al2O3 sample crucibles, and the mass was measured against an empty crucible. Samples were heated from 25 to 1500 °C at a rate of 10 °C/min under Ar at a flow rate of 50 mL/min.

■ ASSOCIATED CONTENT

Supporting Information

The Supporting Information is available free of charge at https://pubs.acs.org/doi/10.1021/acs.chemmater.5c02801.

Additional instrumentation; details on SEM-EDS, XAS, NEXAFS, and ex-situ/in situ HE-XRD instrumentation (PDF)

■ AUTHOR INFORMATION

Corresponding Authors

Matthew B. Dickerson − *Materials and Manufacturing Directorate, Air Force Research Laboratory, Dayton, Ohio 45433, United States;* orcid.org/0000-0003-3000-0290; Email: matthew.dickerson.6@us.af.mil

Nicholas M. Bedford − *Energy and Environment Science & Technology Directorate, Idaho National Laboratory, Idaho Falls, Idaho 83401, United States; Department of Chemistry, Colorado School of Mines, Golden, Colorado 80401, United States;* orcid.org/0000-0002-4424-7094; Email: nicholas.bedford@mines.edu

Timothy L. Pruyn − *Materials and Manufacturing Directorate, Air Force Research Laboratory, Dayton, Ohio 45433, United States*; Email: timothy.pruyn.1@us.af.mil

https://doi.org/10.1021/acs.chemmater.5c02801
Chem. Mater. 2026, 38, 3941−3950

Authors

James F. Ponder, Jr − *Materials and Manufacturing Directorate, Air Force Research Laboratory, Dayton, Ohio 45433, United States; AV Inc., Dayton, Ohio 45432, United States;* orcid.org/0000-0001-8093-1849

Haira G. Hackbarth − *School of Chemical Engineering, University of New South Wales, Sydney, New South Wales 2052, Australia*

Stephanie L. Chua − *School of Chemical Engineering, University of New South Wales, Sydney, New South Wales 2052, Australia*

Yuwei Yang − *School of Chemical Engineering, University of New South Wales, Sydney, New South Wales 2052, Australia*

Nicholas D. Posey − *Materials and Manufacturing Directorate, Air Force Research Laboratory, Dayton, Ohio 45433, United States;* orcid.org/0000-0001-9702-7960

Brandon J. Ackley − *Materials and Manufacturing Directorate, Air Force Research Laboratory, Dayton, Ohio 45433, United States; ARCTOS Technology Solutions, Dayton, Ohio 45432, United States;* orcid.org/0000-0002-8234-3220

Chih-Wen Pao − *National Synchrotron Radiation Research Center, Hsinchu 30076, Taiwan;* orcid.org/0000-0001-7681-4391

Andrey A. Yakovenko − *X-ray Science Division, Advanced Photon Source, Argonne National Laboratory, Lemont, Illinois 60439, United States*

Complete contact information is available at: https://pubs.acs.org/10.1021/acs.chemmater.5c02801

Author Contributions

○J.F.P. and H.G.H. contributed equally.

Notes

The authors declare no competing financial interest.

■ ACKNOWLEDGMENTS

This work was funded by the Air Force Office of Scientific Research under the Aerospace Composites Portfolio (program officer Major Derek Barbee) and Organic Materials Chemistry Portfolio (program officer, Ken Caster) and through FA2386-20-1-4048 and FA2386-22-1-4063. Synthesis and laboratory research at AFRL/RX was performed under contract FA8650-21-F5238 0002 via subtask 188-02B-50. Writing was performed by AV Inc. employees under contract FA8650-21-D-5279. Additional financial support was provided by the Asian Office of Aerospace Research. NEXAFS measurements were performed on the SXR beamline at the Australian Synchrotron, part of ANSTO, funded by the Australian Government, where we kindly acknowledge the technical support and assistance of Dr. Lars Thomsen and Bruce Cowie. We would like to thank Nicolas Trcera and Delphine Vantelon for their assistance at the LUCIA (Soleil) beamline, where Si K-edge measurements of standards were undertaken. The authors thank the experimental facility and the technical services provided by the beamline 44A Quick-scanning X-ray Absorption Spectroscopy of Taiwan Photon source and the National Synchrotron Radiation Research Center (NSRRC), a national user facility supported by the National Science and Technology Council of Taiwan (NSTC), Taiwan (R.O.C.). We also acknowledge the European Synchrotron Radiation Facility (ESRF) for the provision of synchrotron radiation facilities, and we would like to thank Pierre-Olivier Autran for his assistance and support in using the ID11 beamline for ex-situ HE-XRD measurements. In-situ HE-XRD/PDF pyrolysis measurements were performed at 11-ID-C of the Advanced Photon Source, a U.S. Department of Energy (DOE) Office of Science User Facility, operated for the DOE Office of Science by Argonne National Laboratory under Contract No. DE-AC02-06CH11357. Approved for public release.

■ REFERENCES

(1) Colombo, P.; Mera, G.; Riedel, R.; Soraru, G. D. Polymer-derived ceramics: 40 years of research and innovation in advanced ceramics. *J. Am. Ceram. Soc.* **2010**, *93* (7), 1805−1837.

(2) Ackley, B. J.; Martin, K. L.; Key, T. S.; Clarkson, C. M.; Bowen, J. J.; Posey, N. D.; Ponder Jr, J. F.; Apostolov, Z. D.; Cinibulk, M. K.; Pruyn, T. L.; et al. Advances in the Synthesis of Preceramic Polymers for the Formation of Silicon-Based and Ultrahigh-Temperature Non-Oxide Ceramics. *Chem. Rev.* **2023**, *123* (8), 4188−4236.

(3) Chaudhary, R. P.; Parameswaran, C.; Idrees, M.; Rasaki, A. S.; Liu, C.; Chen, Z.; Colombo, P. Additive manufacturing of polymer-derived ceramics: Materials, technologies, properties and potential applications. *Prog. Mater. Sci.* **2022**, *128*, 100969.

(4) Zhou, Y.; Lu, K. Polymer-derived high-temperature nonoxide materials: a review. *Adv. Eng. Mater.* **2023**, *25* (9), 2200967.

(5) Ionescu, E.; Mera, G.; Riedel, R. Polymer-derived ceramics (PDCs): materials design towards applications at ultrahigh-temperatures and in extreme environments. In *Nanotechnology: Concepts, Methodologies, Tools, and Applications*; IGI Global, 2014; pp 1108−1139.

(6) Bouzat, F.; Foucaud, S.; Leconte, Y.; Maître, A.; Lucas, R. From click to ceramic: An efficient way to generate multielement Si/Zr/C clicked-polymer-derived ceramics (cPDC). *Mater. Lett.* **2013**, *106*, 337−340.

(7) Kiessling, L. L. Nobel laureates in Chemistry. *Proceedings of the National Academy of Sciences*: National Academy of Sciences 2023, *120* (35), e2308367120.

(8) Liu, Z.-C.; Zuo, B.; Lu, H.-F.; Wang, M.; Huang, S.; Chen, X.-M.; Lin, B.-P.; Yang, H. A copper (i)-catalyzed azide−alkyne click chemistry approach towards multifunctional two-way shape-memory actuators. *Polym. Chem.* **2020**, *11* (22), 3747−3755.

(9) Wang, X.; Schmidt, F.; Hanaor, D.; Kamm, P. H.; Li, S.; Gurlo, A. Additive manufacturing of ceramics from preceramic polymers: A versatile stereolithographic approach assisted by thiol-ene click chemistry. *Addit. Manuf.* **2019**, *27*, 80−90.

(10) Bowen, J. J.; Mooraj, S.; Goodman, J. A.; Peng, S.; Street, D. P.; Roman-Manso, B.; Davidson, E. C.; Martin, K. L.; Rueschhoff, L. M.; Schiffres, S. N.; et al. Hierarchically porous ceramics via direct writing of preceramic polymer-triblock copolymer inks. *Mater. Today* **2022**, *58*, 71−79.

(11) Hoffmann, M.; Zahedtalaban, M.; Denk, J.; Horcher, A.; Ruckdäschel, H.; Schafföner, S.; Motz, G. Photoinduced thiol-ene "click" chemistry for resource-efficient curing of polysilazane-based coatings and its effects on coating property profile. *Open Ceram.* **2023**, *15*, 100384.

(12) Meldal, M.; Tornøe, C. W. Cu-Catalyzed Azide−Alkyne Cycloaddition. *Chem. Rev.* **2008**, *108* (8), 2952−3015.

(13) Wang, C.; Ikhlef, D.; Kahlal, S.; Saillard, J.-Y.; Astruc, D. Metal-catalyzed azide-alkyne "click" reactions: Mechanistic overview and recent trends. *Coord. Chem. Rev.* **2016**, *316*, 1−20.

(14) Garcia, L.; Maisonneuve, S.; Xie, J.; Guillot, R.; Dorlet, P.; Rivière, E.; Desmadril, M.; Lambert, F.; Policar, C. Sugars to control ligand shape in metal complexes: conformationally constrained glycoligands with a predetermination of stereochemistry and a structural control. *Inorg. Chem.* **2010**, *49* (16), 7282−7288.

(15) Moraes, L. C.; de Souza, G. P.; Fajardo, H. V.; Luz, S. C.; Álvarez, E.; Lloret, F.; Ribeiro-Viana, R. M.; Rojo, J.; Stumpf, H. O.; Figueiredo, R. C.; et al. 1D coordination polymer based on copper (II)-containing tetrameric 1, 2, 3-triazole ligand from click chemistry:

Magnetic and catalytic properties. *Inorg. Chim. Acta* **2019**, *489*, 93−99.
(16) Bouzat, F.; Lucas, R.; Leconte, Y.; Foucaud, S.; Champavier, Y.; Coelho Diogo, C.; Babonneau, F. Formation of ZrC−SiC Composites from the Molecular Scale through the Synthesis of Multielement Polymers. *Materials* **2021**, *14* (14), 3901.
(17) Crowley, J. D.; McMorran, D. A. "Click-triazole" coordination chemistry: Exploiting 1, 4-disubstituted-1, 2, 3-triazoles as ligands. *Top. Heterocycl. Chem.* **2012**, *28*, 31−83.
(18) Kovács, A.; Nemcsok, D. S.; Kocsis, T. Bonding interactions in EDTA complexes. *J. Mol. Struct.:THEOCHEM* **2010**, *950* (1), 93−97.
(19) Maketon, W.; Zenner, C. Z.; Ogden, K. L. Removal efficiency and binding mechanisms of copper and copper− EDTA complexes using polyethyleneimine. *Environ. Sci. Technol.* **2008**, *42* (6), 2124−2129.
(20) Terban, M. W.; Billinge, S. J. Structural analysis of molecular materials using the pair distribution function. *Chem. Rev.* **2022**, *122* (1), 1208−1272.
(21) Chaney, H.; Zhou, Y.; Lu, K. Understanding SiOC atomic structures via synchrotron X-ray and reactive force field potential studies. *Mater. Today Chem.* **2023**, *29*, 101429.
(22) Chua, S. L.; Hackbarth, H. G.; Ponder, J. F., Jr; Posey, N. D.; Yang, Y.; Autran, P.-O.; Dickerson, M. B.; Pruyn, T. L.; Bedford, N. M. Atomic-scale structure elucidation of refractory metal carbides derived from metallocene-based preceramics. *J. Am. Ceram. Soc.* **2025**, *108* (12), No. e70178.
(23) Bedford, N.; Dablemont, C.; Viau, G.; Chupas, P.; Petkov, V. 3-D structure of nanosized catalysts by high-energy X-ray diffraction and reverse Monte Carlo simulations: Study of Ru. *J. Phys. Chem. C* **2007**, *111* (49), 18214−18219.
(24) Liu, L.; Yiu, Y.; Sham, T.; Zhang, L.; Zhang, Y. Electronic structures and optical properties of 6H-and 3C-SiC microstructures and nanostructures from X-ray absorption fine structures, X-ray excited optical luminescence, and theoretical studies. *J. Phys. Chem. C* **2010**, *114* (15), 6966−6975.
(25) Kanazawa, T.; Kitajima, Y.; Yokoyama, T.; Yagi, S.; Imanishi, A.; Ohta, T. Adsorption and decomposition of SiH4 and surface silicide formation on Cu (111) studied by X-ray absorption fine structure spectroscopy. *Surf. Sci.* **1996**, *357*, 160−164.
(26) Hackbarth, H. G.; Key, T. S.; Ackley, B. J.; Opletal, G.; Rawal, A.; Gallington, L.; Yang, Y.; Thomsen, L.; Dickerson, M. B.; Pruyn, T. L.; et al. Uncovering atomic-scale polymer-to-ceramic transformations in SiC polymer derived ceramics from polycarbosilanes. *J. Eur. Ceram. Soc.* **2024**, *44* (4), 1932−1945.
(27) Hackbarth, H. G.; Key, T. S.; Cataldo, T.; Dillingham, I.; Yang, Y.; Dickerson, M. B.; Pruyn, T. L.; Bedford, N. M. Elucidation of Local Ordering and Atomic-Scale Structure in Polymer-Derived SiOC. *ACS Omega* **2025**, *10* (15), 14745−14754.
(28) Lin, Y.-C.; Teng, P.-Y.; Yeh, C.-H.; Koshino, M.; Chiu, P.-W.; Suenaga, K. Structural and Chemical Dynamics of Pyridinic-Nitrogen Defects in Graphene. *Nano Lett.* **2015**, *15* (11), 7408−7413.
(29) Lapteva, L. L.; Fedoseeva, Y. V.; Shlyakhova, E. V.; Makarova, A. A.; Bulusheva, L. G.; Okotrub, A. V. NEXAFS spectroscopy study of lithium interaction with nitrogen incorporated in porous graphitic material. *J. Mater. Sci.* **2019**, *54* (16), 11168−11178.
(30) Tsai, H.; Jan, J.; Chiou, J.; Pong, W.; Tsai, M.-H.; Chang, Y.; Chen, Y.; Yang, Y.; Lai, L.; Wu, J.; et al. Electronic and bonding structures of amorphous Si−C−N thin films by x-ray absorption spectroscopy. *Appl. Phys. Lett.* **2001**, *79* (15), 2393−2395.
(31) Gaur, A.; Shrivastava, B.; Joshi, S. Copper K-edge XANES of Cu (I) and Cu (II) oxide mixtures. In *Journal of Physics: Conference Series*, 2009; IOP Publishing: Vol. *190*, 012084.
(32) Drake, I. J.; Fujdala, K. L.; Baxamusa, S.; Bell, A. T.; Tilley, T. D. Effects of precursor composition on the local structure of Cu dispersed on mesoporous silica: a detailed X-ray absorption spectroscopy study. *J. Phys. Chem. B* **2004**, *108* (48), 18421−18434.
(33) Drake, I. J.; Fujdala, K. L.; Baxamusa, S.; Bell, A. T.; Tilley, T. D. Effects of Precursor Composition on the Local Structure of Cu Dispersed on Mesoporous Silica: A Detailed X-ray Absorption Spectroscopy Study. *J. Phys. Chem. B* **2004**, *108* (48), 18421−18434.
(34) Gaur, A.; Shrivastava, B. D.; Joshi, S. K. Copper K-edge XANES of Cu(I) and Cu(II) oxide mixtures. *Journal of Physics: Conference Series* 2009, *190*(1), 012084.
(35) Buonassisi, T.; Marcus, M. A.; Istratov, A. A.; Heuer, M.; Ciszek, T. F.; Lai, B.; Cai, Z.; Weber, E. R. Analysis of copper-rich precipitates in silicon: Chemical state, gettering, and impact on multicrystalline silicon solar cell material. *J. Appl. Phys.* **2005**, *97* (6), 063503.
(36) Chen, X.; Zhang, X.; Cui, J.; Zhang, Y.; Baranova, E. A.; Wang, Y.; Shu, X.; Qin, Y.; Liu, J.; Wu, Y. Cu3Si-Modified Silicon Nanoparticles Encapsulated within SiO x and Hollow Carbon for Lithium-Ion Battery Anodes. *ACS Appl. Nano Mater.* **2022**, *5* (10), 14275−14284.
(37) Cui, L.; Cui, L.; Li, Z.; Zhang, J.; Wang, H.; Lu, S.; Xiang, Y. A copper single-atom catalyst towards efficient and durable oxygen reduction for fuel cells. *J. Mater. Chem. A* **2019**, *7* (28), 16690−16695.
(38) Zhang, Y.; Ye, S.; Gao, M.; Li, Y.; Huang, X.; Song, J.; Cai, H.; Zhang, Q.; Zhang, J. N-Doped Graphene Supported Cu Single Atoms: Highly Efficient Recyclable Catalyst for Enhanced C−N Coupling Reactions. *ACS Nano* **2022**, *16* (1), 1142−1149.
(39) Lalmi, B.; Chorro, M.; Belkhou, R. High resolution scanning tunnelling microscopy and extended x-ray-absorption fine structure study of the (5× 3) silicide structure on Cu (001). *J. Appl. Phys.* **2013**, *114* (6), 063505.
(40) Bellagamba, M.; Bencivenni, L.; Gontrani, L.; Guidoni, L.; Sadun, C. Tautomerism in liquid 1, 2, 3-triazole: A combined energy-dispersive X-ray diffraction, molecular dynamics, and FTIR study. *Struct. Chem.* **2013**, *24*, 933−943.
(41) Andersen, N. K.; Døssing, H.; Jensen, F.; Vester, B.; Nielsen, P. Duplex and triplex formation of mixed pyrimidine oligonucleotides with stacking of phenyl-triazole moieties in the major groove. *J. Org. Chem.* **2011**, *76* (15), 6177−6187.
(42) Hayes, J. A.; Eccles, K. S.; Coles, S. J.; Lawrence, S. E.; Moynihan, H. A. Supramolecular stacking motifs in the solid state of amide and triazole derivatives of cellobiose. *Carbohydr. Res.* **2014**, *388*, 67−72.
(43) Autthawong, T.; Namsar, O.; Yu, A.; Sarakonsri, T. Cost-effective production of SiO 2/C and Si/C composites derived from rice husk for advanced lithium-ion battery anodes. *J. Mater. Sci.:Mater. Electron.* **2020**, *31*, 9126−9132.
(44) Lu, K.; Chaney, H. New insight into SiOC atomic structure evolution during early stage of pyrolysis. *J. Am. Ceram. Soc.* **2023**, *106* (5), 2737−2743.
(45) Iglesias, M.; Beetstra, D. J.; Knight, J. C.; Ooi, L.-L.; Stasch, A.; Coles, S.; Male, L.; Hursthouse, M. B.; Cavell, K. J.; Dervisi, A.; et al. Novel expanded ring N-heterocyclic carbenes: free carbenes, silver complexes, and structures. *Organometallics* **2008**, *27* (13), 3279−3289.
(46) Amkreutz, M.; Frauenheim, T. Understanding precursor-derived amorphous Si-CN ceramics on the atomic scale. *Phys. Rev. B:Condens. Matter* **2002**, *65* (13), 134113.
(47) Loughney, P. A.; Cuillier, P.; Pruyn, T. L.; Doan-Nguyen, V. Tracking copper nanofiller evolution in polysiloxane during processing into SiOC ceramic. *Appl. Crystallogr.* **2024**, *57* (4), 945−954.
(48) Chupas, P. J.; Chapman, K. W.; Kurtz, C.; Hanson, J. C.; Lee, P. L.; Grey, C. P. A versatile sample-environment cell for non-ambient X-ray scattering experiments. *Appl. Crystallogr.* **2008**, *41* (4), 822−824.

https://doi.org/10.1021/acs.chemmater.5c02801
Chem. Mater. 2026, 38, 3941−3950